Robotica (2005) volume 23, pp. 387–396. © 2005 Cambridge University Press
doi:10.1017/S0263574704000918 Printed in the United Kingdom

Recognizing object surface properties using impedance perception

Ryo Kikuuwe* and Tsuneo Yoshikawa†

(Received in Final Form: July 3, 2004)

SUMMARY

By using the impedance perception algorithm, which we previously proposed, the stiffness matrix that constrains the motion-force relation of a robot's end-effector is calculated in real-time. In this paper, we describe methods of extracting information concerning certain local properties of object surfaces from the stiffness matrix when the end-effector is slid on the surfaces. We develop two algorithms to deal with two classes of surfaces: flat and convex cylindrical surfaces. Since the proposed methods are designed separately from control strategies, they can be used for both autonomous and remote controlled robots. The results of preliminary experiments are presented.

KEYWORDS: Impedance perception; Stiffness matrix; Friction coefficient; Surface normal; Curvature.

1. INTRODUCTION

Humans can perform a wide variety of manipulation tasks in uncertain and unstructured environments. These motor skills are very important, both in everyday circumstances and in manufacturing. However, at the present time, there still remain many difficulties in implementing such motor skills in a robot. One of the requirements of a robot is that it have various perception capabilities. In particular, haptic perception is important to recognize local and dynamic properties of the environment and the physical constraints imposed on the end-effector. This capability can be realized by capabilities of receiving data of position and force, of recognizing the constraint among these signals, and of inferring the physical mechanism that generates this constraint.

Active probing operations using an integrated perception-motor function (Figure 1(a)) allow efficient and accurate haptic perception[1–3]. However, this scheme contains various problems ranging from low level control problems to high level planning problems. Moreover, when a probing operation is performed, the primarily aimed operation has to be suspended. An easier solution is to design a perceptive function as an encapsulated function (Figure 1(b)) which is independent from motor function[4–7]. This is less efficient but has a broader range of applications, for both autonomous and remote-controlled robots. Moreover, it can be used for monitoring human manipulation (Figure 1(c)) in order to analyze human skills[8–10] and to recognize an environment's properties[11]. Research on this kind of scheme has been limited to non-deformable environments by using geometric constraint among objects.

In a previous paper[12], the authors proposed the technique of the *impedance perception* algorithm (IPA), which is of the type shown in Figure 1(b) and Figure 1(c). This technique recognizes constraint imposed on the end-effector based on impedance information that is obtained from the position of the end-effector and the force applied to the end-effector. Experiments have shown that this technique has a potential to be fundamental for real-time and human-like haptic perception.

This paper describes applications of the IPA. When the end-effector is slid on a surface, the stiffness matrix calculated by the IPA contains information on various properties of the surface. This paper describes methods of extracting information regarding certain local properties of surfaces. We develop two algorithms to deal with two classes of surfaces: flat and convex cylindrical surfaces. By the algorithm for flat surfaces, the normal direction, the stiffness coefficient, and the friction coefficient are estimated. By one for cylindrical surfaces, the normal direction, the primary directions, the curvature, the stiffness coefficient, and the friction coefficient are estimated. This kind of information is indispensable for adaptive robots. Flat surface properties are important especially in tasks that require force control on the surface, in such contexts as polishing and drawing. Cylindrical surface properties are also useful because there are many cylindrical objects, such as pipes, bottles, and cans, in our everyday circumstances. Tactile sensors may also be useful for the same purposes[13–14], but there are still difficulties especially regarding durability and wiring complexity, and such sensors are not suitable when the robot interacts with the environment through a tool.

Humans can roughly imagine various properties of objects from even a brief touch. Our main purpose is to implement this capability in a robot, i.e. extracting qualitative information including uncertainty from a small amount of sensor data.

In the rest of this paper, section 2 describes a brief review on the method to calculate the stiffness matrix by using the IPA. The new methods for estimating flat and cylindrical surface properties are explained in sections 3 and 4, respectively. Experiments to test these methods are presented in sections 5 and 6, respectively. Section 7 provides a conclusion.

* Dept. of Mechanical Engineering, Nagoya Institute of Technology, Nagoya, 466-8555 (Japan). E-mail: kikuuwe@ieee.org Corresponding author.
† Dept. of Mechanical Engineering, Kyoto University, Kyoto, 606-8501 (Japan). E-mail: yoshi@mech.kyoto-u.ac.jp

https://doi.org/10.1017/S0263574704000918 Published online by Cambridge University Press

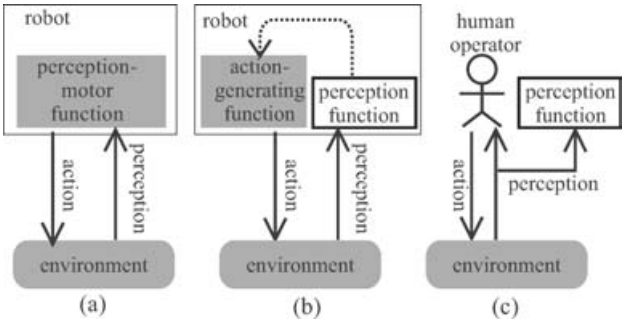


Fig. 1. Perception and motor functions: (a) Integrated perception-motor function. (b) Encapsulated perception function. (c) Encapsulated perception function for monitoring actions of a human operator.

2. STIFFNESS MATRIX PROVIDED BY THE IPA

In the IPA[12], the position of the robot's end-effector, $\boldsymbol{p}(t) \in \mathcal{R}^3$, and the force applied to the end-effector from the environment, $\boldsymbol{f}(t) \in \mathcal{R}^3$, are fitted to a linear equation. The recursive least squares method with a forgetting factor is employed for estimating the coefficients. The uncertainties of the estimates are determined based on the residual fitting error and excitation of the position data.

The fitting equation is given as follows:

$$\boldsymbol{f}(t) = \boldsymbol{c} + \boldsymbol{K}\,\boldsymbol{p}(t) + \boldsymbol{B}\,\dot{\boldsymbol{p}}(t) + \boldsymbol{M}\,\ddot{\boldsymbol{p}}(t), \tag{1}$$

where $\boldsymbol{K}$, $\boldsymbol{B}$, and $\boldsymbol{M} \in \mathcal{R}^{3\times3}$ are the matrices of stiffness, viscosity, and inertia, respectively, that the robot perceives. These matrices are dependent on the dynamic properties of the end-effector and the environment, and on the contact configuration between them. $\boldsymbol{c} \in \mathcal{R}^3$ is a constant vector which corresponds to the equilibrium point of the stiffness, a force bias resulting from the gravitation, and etc. By using the Laplace transform and the bilinear transform, (1)'s discrete-time approximation is written as follows:

$$\boldsymbol{\phi}_k = \boldsymbol{\Theta}^T \boldsymbol{\psi}_k \tag{2}$$

$$\boldsymbol{\phi}_k \triangleq \boldsymbol{f}_k + 2\boldsymbol{f}_{k-1} + \boldsymbol{f}_{k-2} \in \mathcal{R}^3 \tag{3}$$

$$\boldsymbol{\psi}_k \triangleq \begin{bmatrix} 1 & \boldsymbol{p}_k{}^T & \boldsymbol{p}_{k-1}{}^T & \boldsymbol{p}_{k-2}{}^T \end{bmatrix}^T \in \mathcal{R}^{10} \tag{4}$$

$$\boldsymbol{\Theta} \triangleq \begin{bmatrix} 4\boldsymbol{c}^T \\ \boldsymbol{K}^T + 2\boldsymbol{B}^T/T + 4\boldsymbol{M}^T/T^2 \\ 2\boldsymbol{K}^T - 8\boldsymbol{M}^T/T^2 \\ \boldsymbol{K}^T - 2\boldsymbol{B}^T/T + 4\boldsymbol{M}^T/T^2 \end{bmatrix} \in \mathcal{R}^{10\times3}, \tag{5}$$

where T is the sampling period and the subscript k denotes the value of the variable at time kT.

At time kT, the weighted sum-of-products matrix of the residual fitting errors is written as

$$\begin{aligned} \boldsymbol{J}_k(\boldsymbol{\Theta}) &\triangleq \sum_{i=i_0}^{k} w_{k,i}(\boldsymbol{\phi}_i - \boldsymbol{\Theta}^T\boldsymbol{\psi}_i)(\boldsymbol{\phi}_i - \boldsymbol{\Theta}^T\boldsymbol{\psi}_i)^T \\ &= \boldsymbol{\Theta}^T\boldsymbol{R}_k\boldsymbol{\Theta} - \boldsymbol{Q}_k{}^T\boldsymbol{\Theta} - \boldsymbol{\Theta}^T\boldsymbol{Q}_k + \boldsymbol{F}_k, \end{aligned} \tag{6}$$

where $\{w_{k,i}\}_{i_0\le i\le k}$ denotes the weighting sequence at time kT, i_0 denotes the time index at which the calculation starts, $\boldsymbol{R}_k \triangleq \sum_{i=i_0}^{k} w_{k,i}\boldsymbol{\psi}_i\boldsymbol{\psi}_i{}^T$, $\boldsymbol{Q}_k \triangleq \sum_{i=i_0}^{k} w_{k,i}\boldsymbol{\psi}_i\boldsymbol{\phi}_i{}^T$, and $\boldsymbol{F}_k \triangleq \sum_{i=i_0}^{k} w_{k,i}\boldsymbol{\phi}_i\boldsymbol{\phi}_i{}^T$. The weighting is designed depending on the speed of the motion of the end-effector, so that the estimated values are updated rapidly during high-speed motion.

When $\boldsymbol{R}_k{}^{-1}$ exists, (6) is transformed as follows:

$$\boldsymbol{J}_k(\boldsymbol{\Theta}) = (\boldsymbol{\Theta} - \hat{\boldsymbol{\Theta}}_k)^T\boldsymbol{R}_k(\boldsymbol{\Theta} - \hat{\boldsymbol{\Theta}}_k) + \boldsymbol{S}_k \tag{7}$$

$$\hat{\boldsymbol{\Theta}}_k \triangleq \boldsymbol{R}_k{}^{-1}\boldsymbol{Q}_k \in \mathcal{R}^{10\times3} \tag{8}$$

$$\boldsymbol{S}_k \triangleq \boldsymbol{F}_k - \boldsymbol{Q}_k{}^T\boldsymbol{R}_k{}^{-1}\boldsymbol{Q}_k \in \mathcal{R}^{3\times3}. \tag{9}$$

Since $\boldsymbol{R}_k$ is positive definite, $\boldsymbol{J}_k(\boldsymbol{\Theta}) \succeq \boldsymbol{J}_k(\hat{\boldsymbol{\Theta}}_k) = \boldsymbol{S}_k$ is satisfied for any $\boldsymbol{\Theta}$ ($\boldsymbol{X} \succeq \boldsymbol{Y}$ means that $\boldsymbol{X} - \boldsymbol{Y}$ is positive semi-definite). Therefore, $\hat{\boldsymbol{\Theta}}_k$ is defined as the estimate of $\boldsymbol{\Theta}$ at time kT.

Since $\boldsymbol{J}_k(\boldsymbol{\Theta}) \succeq \boldsymbol{S}_k$, $\boldsymbol{S}_k$ is the minimum of $\boldsymbol{J}_k(\boldsymbol{\Theta})$ in the partial order relation "$\preceq$". By normalizing $\boldsymbol{J}_k(\boldsymbol{\Theta})$ with respect to its minimum $\boldsymbol{S}_k$, a generalized distance measure from $\hat{\boldsymbol{\Theta}}_k$ to a given $\boldsymbol{\Theta}$ can be defined as

$$\begin{aligned} D_{\Theta,k}(\boldsymbol{\Theta}) &= \mathrm{tr}\left[\boldsymbol{S}_k^{-\frac{1}{2}}(\boldsymbol{J}_k(\boldsymbol{\Theta}) - \boldsymbol{S}_k)\boldsymbol{S}_k^{-\frac{1}{2}}\right] \\ &= \mathrm{tr}\left[\boldsymbol{S}_k^{-\frac{1}{2}}(\boldsymbol{\Theta} - \hat{\boldsymbol{\Theta}}_k)^T\boldsymbol{R}_k(\boldsymbol{\Theta} - \hat{\boldsymbol{\Theta}}_k)\boldsymbol{S}_k^{-\frac{1}{2}}\right] \\ &= \mathrm{vec}\left[\boldsymbol{\Theta} - \hat{\boldsymbol{\Theta}}_k\right]^T\left(\boldsymbol{S}_k{}^{-1} \otimes \boldsymbol{R}_k\right)\mathrm{vec}\left[\boldsymbol{\Theta} - \hat{\boldsymbol{\Theta}}_k\right]. \end{aligned} \tag{10}$$

Here, $\boldsymbol{X} \otimes \boldsymbol{Y}$ denotes the Kronecker product of $\boldsymbol{X}$ ($\in \mathcal{R}^{m\times n}$) and $\boldsymbol{Y}$ ($\in \mathcal{R}^{p\times q}$), which is defined as

$$\boldsymbol{X} \otimes \boldsymbol{Y} = \begin{bmatrix} x_{11}\boldsymbol{Y} & \cdots & x_{1n}\boldsymbol{Y} \\ \vdots & \ddots & \vdots \\ x_{m1}\boldsymbol{Y} & \cdots & x_{mn}\boldsymbol{Y} \end{bmatrix} \in \mathcal{R}^{mp\times nq},$$

and $\mathrm{vec}[\boldsymbol{X}]$ denotes the vectorization of $\boldsymbol{X}$ ($\in \mathcal{R}^{m\times n}$), which is defined as

$$\mathrm{vec}[\boldsymbol{X}] = \begin{bmatrix} \boldsymbol{x}_1{}^T & \cdots & \boldsymbol{x}_n{}^T \end{bmatrix}^T \in \mathcal{R}^{mn},$$

where $\boldsymbol{x}_i$ ($i = 1, \ldots, n$) are the i-th column vector of $\boldsymbol{X}$. In (10) we used the following relations:

$$\mathrm{tr}[\boldsymbol{X}^T\boldsymbol{Y}] = \mathrm{vec}[\boldsymbol{X}]^T\,\mathrm{vec}[\boldsymbol{Y}]$$

$$\mathrm{vec}[\boldsymbol{X}\boldsymbol{Y}\boldsymbol{Z}] = (\boldsymbol{Z}^T \otimes \boldsymbol{X})\,\mathrm{vec}[\boldsymbol{Y}],$$

where $\boldsymbol{X}$, $\boldsymbol{Y}$, and $\boldsymbol{Z}$ are matrices of appropriate size. We refer to the set of $\boldsymbol{\Theta}$s which satisfy $D_{\Theta,k}(\boldsymbol{\Theta}) \le 1$ as the uncertainty ellipsoid of $\hat{\boldsymbol{\Theta}}_k$. This ellipsoid is a subset of the 30-dimensional space $\{\boldsymbol{\Theta} \in \mathcal{R}^{10\times3}\}$.

If $\boldsymbol{p}(t)$ in (1) is substituted by the true position measured by the sensors, the estimated impedance can become very unstable in nearly rigid contact situations. This problem is avoided by implementing a computer-simulated virtual

https://doi.org/10.1017/S0263574704000918 Published online by Cambridge University Press

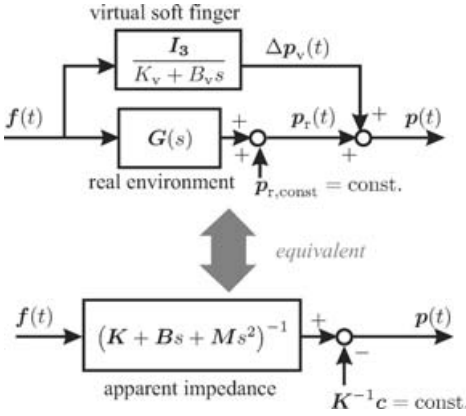


Fig. 2. The virtual soft finger (VSF), the real environment, and the apparent impedance estimated through the VSF.

soft cover around the real end-effector. The displacement of the *virtual soft finger* (VSF), $\Delta \boldsymbol{p}_v(t)$, is simulated by solving $\boldsymbol{f}(t) = K_v \Delta \boldsymbol{p}_v(t) + B_v \Delta \dot{\boldsymbol{p}}_v(t)$, where K_v and B_v are design parameters which are scalars representing the stiffness and viscosity coefficients of the VSF, and $\boldsymbol{f}(t)$ is the force observed by the sensor. The position of the VSF is determined by $\boldsymbol{p}(t) = \boldsymbol{p}_r(t) + \Delta \boldsymbol{p}_v(t)$, where $\boldsymbol{p}_r(t)$ denotes the real position observed by the sensors. By substituting $\boldsymbol{p}(t)$ in (1) with the virtual position, the estimates are stabilized even in rigid contact states.

Figure 2 shows the relation among the VSF, the real environment, and the impedance model (1). In this figure, $\boldsymbol{G}(s)$ denotes the transfer function of the real environment from force to position, $\boldsymbol{p}_{r,const}$ denotes the integral constant, and $\boldsymbol{I}_3$ denotes the 3×3 identity matrix. As is seen in this figure, the relation between the dynamics of the real environment and the apparent impedance $\{\boldsymbol{c}, \boldsymbol{K}, \boldsymbol{B}, \boldsymbol{M}\}$ is described by

$$(\boldsymbol{K} + \boldsymbol{B}s + \boldsymbol{M}s^2)^{-1} = \boldsymbol{G}(s) + \frac{\boldsymbol{I}_3}{K_v + B_v s} \tag{11}$$

$$\boldsymbol{K}^{-1}\boldsymbol{c} = -\boldsymbol{p}_{r,const}. \tag{12}$$

The impedance estimated through the VSF is different from that of the real environment. Instead, it corresponds to that of the serial-coupled system of the real environment and the VSF. The main purpose of the IPA is not an accurate measurement but a qualitative recognition of the constraint distribution over directions. Therefore, estimation through the VSF can be seen as a natural solution, which is analogous to the human's perception of constraint through soft fingers or soft tools. In a passive environment, the theoretical upper bound of stiffness coefficients obtained through the VSF is K_v.

According to relation (5), the estimate of the stiffness matrix $\boldsymbol{K}$ is obtained by $\hat{\boldsymbol{K}}_k \triangleq \hat{\boldsymbol{\Theta}}_k^T \boldsymbol{T}$ where

$$\boldsymbol{T} \triangleq \begin{bmatrix} \boldsymbol{o}_3 & \frac{1}{4}\boldsymbol{I}_3 & \frac{1}{4}\boldsymbol{I}_3 & \frac{1}{4}\boldsymbol{I}_3 \end{bmatrix}^T \in \mathcal{R}^{10\times 3}. \tag{13}$$

Here, $\boldsymbol{o}_3$ denotes the 3-dimensional zero vector. The projection of the ellipsoid $D_{\Theta,k}(\boldsymbol{\Theta}) \leq 1$ (in the 30-dimensional space $\{\boldsymbol{\Theta} \in \mathcal{R}^{10\times 3}\}$) onto the 9-dimensional subspace $\{\boldsymbol{K} \in \mathcal{R}^{3\times 3}\}$ can be given by

$$D_k(\boldsymbol{K}) \triangleq \mathrm{vec}[\boldsymbol{K} - \hat{\boldsymbol{K}}_k]^T \boldsymbol{\Pi}_k^{-1} \mathrm{vec}[\boldsymbol{K} - \hat{\boldsymbol{K}}_k] \leq 1, \tag{14}$$

or equivalently,

$$\mathrm{vec}[\boldsymbol{K} - \hat{\boldsymbol{K}}_k]\mathrm{vec}[\boldsymbol{K} - \hat{\boldsymbol{K}}_k]^T \preceq \boldsymbol{\Pi}_k, \tag{15}$$

where $\boldsymbol{\Pi}_k \triangleq \boldsymbol{P}_k \otimes \boldsymbol{S}_k$ and $\boldsymbol{P}_k \triangleq \boldsymbol{T}^T \boldsymbol{R}_k{}^{-1} \boldsymbol{T}$. This represents the uncertainty ellipsoid of $\hat{\boldsymbol{K}}_k$, and is denoted by $\hat{\boldsymbol{\mathcal{E}}}_k$. $D_k(\boldsymbol{K})$ is a generalized distance from $\hat{\boldsymbol{K}}_k$ to $\boldsymbol{K}$.

3. RECOGNIZING FLAT SURFACE PROPERTIES

When the end-effector is in a kinetic friction state on a single flat surface, the stiffness matrix provided by the IPA contains information not only on the stiffness coefficient and on the normal direction, but also on the friction coefficient. This section explains a method to extract information on these properties.

An analytical derivation shows conditions which are supposed to be satisfied by the stiffness matrix in a situation in which the end-effector is slid on a flat surface. However, the stiffness matrix $\hat{\boldsymbol{K}}$, provided by the IPA, does not generally satisfy this condition. Therefore, a calculation is needed to find a new stiffness matrix which is theoretically consistent with the situation and is sufficiently close to $\hat{\boldsymbol{K}}$. Moreover, an ellipsoidal uncertainty bound accompanied by the new estimate has to be defined. The surface properties are obtained based on the new stiffness matrix and its accompanying uncertainty ellipsoid.

Hereafter, the position of the end-effector is substituted by the virtual position $\boldsymbol{p}(t)$ not by the real position $\boldsymbol{p}_r(t)$. The subscripts to denote the time index (e.g., k and i) are dropped unless required for clarity.

3.1. Stiffness matrix and flat surface properties

Let $\boldsymbol{n}$ denote the normal direction and $\boldsymbol{t}$ denote one of the tangential directions in which the friction force acts. $\boldsymbol{n}$ and $\boldsymbol{t}$ are orthogonal to each other. Let $\boldsymbol{U} \triangleq [\boldsymbol{n}, \boldsymbol{t}, \boldsymbol{n} \times \boldsymbol{t}]$ be defined, then $\boldsymbol{U}$ is a 3×3 rotation matrix. Let $\boldsymbol{p}$ $(\in \mathcal{R}^3)$ be the position of the end-effector, and $\boldsymbol{f}$ $(\in \mathcal{R}^3)$ be the force applied from the end-effector to the environment. Between the position and force, there are two relations. The stiffness in the surface normal direction causes the relation $\boldsymbol{n}^T \delta \boldsymbol{f} = \kappa(\boldsymbol{n}^T \delta \boldsymbol{p})$, and the Coulomb friction causes the relation $\boldsymbol{t}^T \delta \boldsymbol{f} = \mu(\boldsymbol{n}^T \delta \boldsymbol{f})$. Here, δ denotes a small change in the associated variable and κ and μ are the stiffness and friction coefficients, respectively, of the surface. These relations are rewritten as $\delta \boldsymbol{f} = \boldsymbol{K} \delta \boldsymbol{p}$ by using

$$\boldsymbol{K} = \boldsymbol{U} \begin{bmatrix} \kappa & 0 & 0 \\ \kappa\mu & 0 & 0 \\ 0 & 0 & 0 \end{bmatrix} \boldsymbol{U}^T. \tag{16}$$

The above shows that the force-position relation in a kinetic friction state on a flat surface is determined by matrix

https://doi.org/10.1017/S0263574704000918 Published online by Cambridge University Press

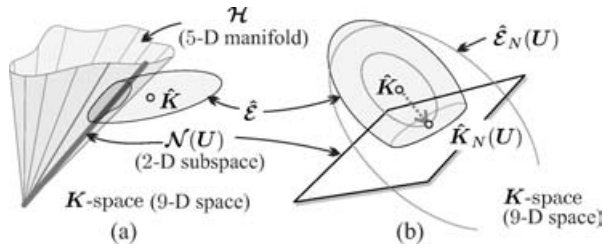


Fig. 3. Inclusive relationship among subsets of $\{\boldsymbol{K} \in \mathcal{R}^{3\times3}\}$.

$\boldsymbol{K}$ in (16). Since $\boldsymbol{K}$ in (16) is non-symmetric, it is not a stiffness matrix in a generally accepted sense of the term. However, it has been known that the stiffness matrix of a system involving friction, such as bearings, can become non-symmetric, and even in these cases the matrix has been referred to as the stiffness matrix[15–16]. We therefore refer to $\boldsymbol{K}$ as a stiffness matrix despite its being non-symmetric throughout this paper.

Let $\mathcal{N}(\boldsymbol{U})$ be a set of $\boldsymbol{K}$s which can be expressed by (16) using a given $\boldsymbol{U}$, and $\mathcal{H}$ be the union of all $\mathcal{N}(\boldsymbol{U})$s. $\mathcal{N}(\boldsymbol{U})$ constitutes a 2-dimensional subspace of $\{\boldsymbol{K} \in \mathcal{R}^{3\times3}\}$, and $\mathcal{H}$ constitutes a 5-dimensional manifold in $\{\boldsymbol{K} \in \mathcal{R}^{3\times3}\}$, as illustrated in Figure 3.

3.2. New estimate $\hat{\mathcal{E}}_N(\boldsymbol{U})$ with respect to a given $\boldsymbol{U}$

Generally $\hat{\boldsymbol{K}}$, which is provided by the IPA, is not an element of $\mathcal{H}$. Therefore, it is necessary to find an element of $\mathcal{H}$ which is close to $\hat{\boldsymbol{K}}$, and to define its accompanying uncertainty ellipsoid.

We derive the element of $\mathcal{N}(\boldsymbol{U})$ that minimizes $D(\boldsymbol{K})$, hereafter $\hat{\boldsymbol{K}}_N(\boldsymbol{U})$, with a given $\boldsymbol{U}$. By letting $\boldsymbol{N} = \boldsymbol{n} \otimes [\boldsymbol{n}, \boldsymbol{t}] \in \mathcal{R}^{9\times2}$, $\boldsymbol{K} \in \mathcal{N}$ can be written as $\mathrm{vec}\boldsymbol{K} = \boldsymbol{N}\boldsymbol{\xi}$, $\boldsymbol{\xi} \triangleq [\kappa, \mu\kappa]$. Under the condition $\boldsymbol{K} \in \mathcal{N}$, $D(\boldsymbol{K})$ can be rewritten as

$$D(\boldsymbol{K}) = (\boldsymbol{\xi} - \hat{\boldsymbol{\xi}}_N)^T \boldsymbol{V_N}^{-1}(\boldsymbol{\xi} - \hat{\boldsymbol{\xi}}_N) + \hat{D}_N \tag{17}$$

$$\hat{\boldsymbol{\xi}}_N \triangleq \boldsymbol{V_N}\boldsymbol{N}^T\boldsymbol{\Pi}^{-1}\mathrm{vec}[\hat{\boldsymbol{K}}] \tag{18}$$

$$\hat{D}_N \triangleq \mathrm{vec}[\hat{\boldsymbol{K}}]^T\boldsymbol{\Pi}^{-1}\mathrm{vec}[\hat{\boldsymbol{K}}] - \hat{\boldsymbol{\xi}}_N^T\boldsymbol{V_N}\boldsymbol{N}^T\boldsymbol{\Pi}^{-1}\mathrm{vec}[\hat{\boldsymbol{K}}], \tag{19}$$

where $\boldsymbol{V_N} \triangleq (\boldsymbol{N}^T\boldsymbol{\Pi}^{-1}\boldsymbol{N})^{-1}$. $\hat{\boldsymbol{\xi}}_N$ corresponds to $\hat{\boldsymbol{K}}_N$ in the sense that $\mathrm{vec}[\hat{\boldsymbol{K}}_N] = \boldsymbol{N}\hat{\boldsymbol{\xi}}_N$, and $\hat{D}_N$ is the generalized distance between $\hat{\boldsymbol{K}}_N$ and $\hat{\boldsymbol{K}}$. Note that $\hat{D}_N$, $\boldsymbol{V_N}$ and $\hat{\boldsymbol{\xi}}_N$ are functions of $\boldsymbol{U}$.

The uncertainty ellipsoid accompanied by $\hat{\boldsymbol{K}}_N(\boldsymbol{U})$ can be defined by moving $\hat{\mathcal{E}}$ from $\hat{\boldsymbol{K}}$ to $\hat{\boldsymbol{K}}_N$, and magnifying it according to $\hat{D}_N$. This new ellipsoidal bound, to be denoted by $\hat{\mathcal{E}}_N(\boldsymbol{U})$, is represented by an inequality

$$\mathrm{vec}[\boldsymbol{K} - \hat{\boldsymbol{K}}_N]^T\boldsymbol{\Pi}^{-1}\mathrm{vec}[\boldsymbol{K} - \hat{\boldsymbol{K}}_N] \le 1 + \hat{D}_N. \tag{20}$$

Considering (17), the cross-section of the ellipsoid $\hat{\mathcal{E}}_N(\boldsymbol{U})$ with the plane $\mathcal{N}(\boldsymbol{U})$ is an ellipsoid represented by

$$(\boldsymbol{\xi} - \hat{\boldsymbol{\xi}}_N)^T \boldsymbol{V_N}^{-1}(\boldsymbol{\xi} - \hat{\boldsymbol{\xi}}_N) \le 1 + \hat{D}_N. \tag{21}$$

Note that (20) and (21) are equivalent to the followings respectively:

$$\mathrm{vec}[\boldsymbol{K} - \hat{\boldsymbol{K}}_N]\mathrm{vec}[\boldsymbol{K} - \hat{\boldsymbol{K}}_N]^T \preceq (1 + \hat{D}_N)\boldsymbol{\Pi} \tag{22}$$

$$(\boldsymbol{\xi} - \hat{\boldsymbol{\xi}}_N)(\boldsymbol{\xi} - \hat{\boldsymbol{\xi}}_N)^T \preceq (1 + \hat{D}_N)\boldsymbol{V_N}. \tag{23}$$

Hereafter, ${}^{nn}\xi$ and ${}^{tn}\xi$ denote the 1st and 2nd elements of $\boldsymbol{\xi}$, respectively, and ${}^{nn,nn}V_N$ and ${}^{tn,tn}V_N$ denote the (1, 1)-th and (2, 2)-th elements of $\boldsymbol{V_N}$, respectively.

3.3. Consistency evaluation of $\hat{\mathcal{E}}_N(\boldsymbol{U})$

When a given $\boldsymbol{U}$ is close to the true value, the ellipsoid $\hat{\mathcal{E}}_N(\boldsymbol{U})$ must be consistent with a kinetic friction state on a flat surface whose normal direction is $\boldsymbol{n}$. Equation (16) is a necessary condition, but moreover, κ must be reliably positive. As well, the IPA usually provides estimates with small uncertainties in directions in which the position variance is large. This direction is usually close to the direction of motion, which is close to $\boldsymbol{t}$, and thus $\boldsymbol{K}\boldsymbol{t} = (\boldsymbol{t}^T \otimes \boldsymbol{I}_3)\mathrm{vec}[\boldsymbol{K}] = \boldsymbol{o}_3$ has to be reliably satisfied. Based on this consideration, a maximization criterion for evaluating the consistency of $\hat{\mathcal{E}}_N(\boldsymbol{U})$ can be given as follows:

$$\Phi_N(\boldsymbol{U}) = \Phi_{Nn}(\boldsymbol{U})\Phi_{Nt}(\boldsymbol{U}) \tag{24}$$

$$\Phi_{Nn}(\boldsymbol{U}) \triangleq \frac{\max(0, {}^{nn}\hat{\xi}_N(\boldsymbol{U}))^2}{(1 + \hat{D}_N(\boldsymbol{U}))^{nn,nn}V_N(\boldsymbol{U})} \tag{25}$$

$$\Phi_{Nt}(\boldsymbol{U}) \triangleq \left(\mathrm{tr}\left[\frac{(\boldsymbol{t}^T \otimes \boldsymbol{I}_3)\boldsymbol{\Pi}^{-1}(\boldsymbol{t}^T \otimes \boldsymbol{I}_3)}{(1 + \hat{D}_N(\boldsymbol{U}))}\right]\right)^{-1}. \tag{26}$$

The function $\Phi_{Nn}(\boldsymbol{U})$ is a reliability measure for condition $\kappa = {}^{nn}\xi \gg 0$. Under condition 23, ${}^{nn}\xi$ satisfies

$$({}^{nn}\xi - {}^{nn}\hat{\xi}_N(\boldsymbol{U}))^2 \le (1 + \hat{D}_N(\boldsymbol{U}))^{nn,nn}V_N(\boldsymbol{U}). \tag{27}$$

This shows that $\kappa \gg 0$ is reliably satisfied when $\Phi_{Nn}(\boldsymbol{U})$ is large. On the other hand, $\Phi_{Nn}(\boldsymbol{U})$ is a reliability measure for condition $(\boldsymbol{t}^T \otimes \boldsymbol{I}_3)\mathrm{vec}[\boldsymbol{K}] = \boldsymbol{o}_3$.

By finding $\boldsymbol{U}$ which maximizes $\Phi_N(\boldsymbol{U})$, the estimate of $\boldsymbol{U}$, to be denoted by $\hat{\boldsymbol{U}}$, is obtained. The steepest gradient method is employed to obtain $\hat{\boldsymbol{U}}$.

3.4. Estimating κ and μ

Once $\hat{\boldsymbol{U}}$ is obtained, the final estimates of κ and μ are given by

$$\hat{\kappa} \triangleq {}^{nn}\hat{\xi}_N(\hat{\boldsymbol{U}}) \tag{28}$$

$$\hat{\mu} \triangleq {}^{tn}\hat{\xi}_N(\hat{\boldsymbol{U}})/{}^{nn}\hat{\xi}_N(\hat{\boldsymbol{U}}). \tag{29}$$

The uncertainty regions of $\hat{\kappa}$ and $\hat{\mu}$ are given by

$$(\kappa - \hat{\kappa})^2 \le (1 + \hat{D}_N(\hat{\boldsymbol{U}}))({}^{nn,nn}V_N(\hat{\boldsymbol{U}})) \tag{30}$$

$$(\mu - \hat{\mu})^2 \le (1 + \hat{D}_N(\hat{\boldsymbol{U}}))({}^{tn,tn}V_N(\hat{\boldsymbol{U}}))/\hat{\kappa}^2, \tag{31}$$

respectively.

https://doi.org/10.1017/S0263574704000918 Published online by Cambridge University Press

4. RECOGNIZING CYLINDRICAL SURFACE PROPERTIES

This section describes a method to estimate several properties of a cylindrical surface in a situation in which the end-effector is in a kinetic friction on the surface. This method can be realized in a way similar to that described in the previous section.

An analytical derivation shows conditions which are supposed to be satisfied by the stiffness matrix in a situation in which the end-effector is slid on a cylindrical surface. However, the stiffness matrix $\hat{\boldsymbol{K}}$, provided by the IPA, does not generally satisfy this condition. Therefore, a calculation is needed to determine a new stiffness matrix which is theoretically consistent with the situation and is sufficiently close to $\hat{\boldsymbol{K}}$. Moreover, an uncertainty ellipsoid accompanied by this new estimate must be defined. The surface properties are obtained based on the new stiffness matrix and its accompanying uncertainty ellipsoid.

4.1. Stiffness matrix and cylindrical surface properties

Let $\hat{\boldsymbol{p}}$ denote the center of gravity of positions that the IPA has used to calculate $\hat{\boldsymbol{K}}$. This is written as

$$\hat{\boldsymbol{p}} = \frac{\sum_{i=i_0}^{k} w_{k,i}\, \boldsymbol{p}_i}{\sum_{i=i_0}^{k} w_{k,i}}. \tag{32}$$

$\hat{\boldsymbol{K}}$ can be viewed as the stiffness matrix at position $\hat{\boldsymbol{p}}$. When the end-effector is slid on an object, $\hat{\boldsymbol{p}}$ is usually located below the surface of the object. As shown in Figure 4, let us define $\boldsymbol{p}_U$ as the closest point of $\hat{\boldsymbol{p}}$ on the surface, and let $\boldsymbol{n}$, $\boldsymbol{t}$, and $\boldsymbol{v}$ be orthonormal vectors which represent the normal direction, the primary direction with the minimum curvature, and the primary direction with the maximum curvature, at $\hat{\boldsymbol{p}}$, respectively. Let Σ_U be the coordinate system with axes $\{\boldsymbol{n}, \boldsymbol{t}, \boldsymbol{v}\}$ and origin $\boldsymbol{p}_U$. The attitude of Σ_U is expressed by a 3×3 rotation matrix $\boldsymbol{U} \triangleq [\boldsymbol{n}, \boldsymbol{t}, \boldsymbol{v}]$.

We formulate the force-position relation in the neighborhood of $\hat{\boldsymbol{p}}$. Let $\boldsymbol{p}$ denote the position of the end-effector and $\boldsymbol{f}$ denote the force applied to the surface from the end-effector. Let ${}^U\boldsymbol{p} = [{}^n\boldsymbol{p}, {}^t\boldsymbol{p}, {}^v\boldsymbol{p}]^T$ and ${}^U\boldsymbol{f} = [{}^n\boldsymbol{f}, {}^t\boldsymbol{f}, {}^v\boldsymbol{f}]^T$ denote position $\boldsymbol{p}$ and force $\boldsymbol{f}$, respectively, expressed relative to Σ_U. Vectors ${}^U\boldsymbol{p}$ and ${}^U\boldsymbol{f}$ are related to $\boldsymbol{p}$ and $\boldsymbol{f}$ by $\boldsymbol{p} = \boldsymbol{U}({}^U\boldsymbol{p}) + \boldsymbol{p}_U$ and $\boldsymbol{f} = \boldsymbol{U}({}^U\boldsymbol{f}) + \boldsymbol{f}_{\text{weight}}$, where $\boldsymbol{f}_{\text{weight}}$ is the gravitational force on the end-effector. When the position $\hat{\boldsymbol{p}}$ is expressed relative to Σ_U, it is written as ${}^U\hat{\boldsymbol{p}} = [{}^n\hat{p}, 0, 0]^T$. As shown in Figure 4, let θ be the angle between the surface normal at $\boldsymbol{p}$ and that at $\boldsymbol{p}_U$, N be the normal force applied to the surface at $\boldsymbol{p}$, R be the curvature radius, and κ be the stiffness of the surface. Then, since $\boldsymbol{p}$ is at a depth of N/κ from the surface, ${}^np$ and ${}^vp$ are written as

$$\begin{bmatrix} {}^np \\ {}^vp \end{bmatrix} = \begin{bmatrix} R(1-\cos\theta) + N/\kappa\cos\theta \\ R\sin\theta - N/\kappa\sin\theta \end{bmatrix}. \tag{33}$$

Let α be the angle between the friction direction and $\boldsymbol{t}$-direction at position $\boldsymbol{p}$, as shown in Figure 4, and let μ be the friction coefficient of the surface. Then, since the magnitude

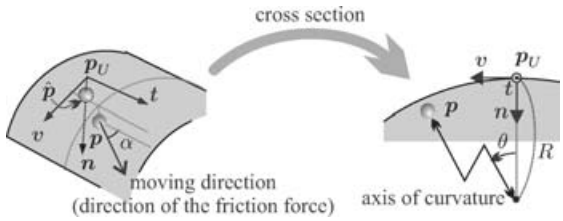


Fig. 4. Sliding on a cylindrical surface.

of the friction force is μN, ${}^U\boldsymbol{f}$ can be written as

$$\begin{bmatrix} {}^nf \\ {}^tf \\ {}^vf \end{bmatrix} = \begin{bmatrix} N(\cos\theta + \mu\sin\alpha\sin\theta) \\ N\mu\cos\alpha \\ N(-\sin\theta + \mu\sin\alpha\cos\theta) \end{bmatrix}. \tag{34}$$

Eliminating θ and N from (33) and (34) yields

$${}^nf = \kappa'((R - {}^np) + ({}^vp)\mu\sin\alpha) \tag{35}$$

$${}^tf = \kappa'\mu\cos\alpha\sqrt{(R-{}^np)^2 + ({}^vp)^2} \tag{36}$$

$${}^vf = \kappa'\left((R-{}^np)\mu\sin\alpha - ({}^vp)\right), \tag{37}$$

where $\kappa' \triangleq \kappa(R/\sqrt{(R-{}^np)^2 + ({}^vp)^2} - 1)$. The stiffness matrix at position $\boldsymbol{p}_U$ is derived as

$$\begin{aligned} \boldsymbol{K} &= \boldsymbol{U}((\partial^U\boldsymbol{f}/\partial^U\boldsymbol{p})|_{{}^v\boldsymbol{p}={}^v\hat{\boldsymbol{p}}})\boldsymbol{U}^T \\ &= \boldsymbol{U}\begin{bmatrix} \kappa & 0 & \kappa\mu\sin\alpha({}^n\hat{p})/(R-{}^n\hat{p}) \\ \kappa\mu\cos\alpha & 0 & 0 \\ \kappa\mu\sin\alpha & 0 & -\kappa({}^n\hat{p})/(R-{}^n\hat{p}) \end{bmatrix}\boldsymbol{U}^T \end{aligned}. \tag{38}$$

Let the elements of $\boldsymbol{U}^T\boldsymbol{K}\boldsymbol{U}$ be denoted by ${}^{nn}\lambda$ ($\triangleq \boldsymbol{n}^T\boldsymbol{K}\boldsymbol{n}$), ${}^{nt}\lambda$ ($\triangleq \boldsymbol{n}^T\boldsymbol{K}\boldsymbol{t}$), and so on. Then, (38) shows that a stiffness matrix obtained in this situation is supposed to satisfy the following conditions:

$${}^{nt}\lambda = {}^{tt}\lambda = {}^{vt}\lambda = {}^{tv}\lambda = 0 \tag{39}$$

$$({}^{vn}\lambda)({}^{vv}\lambda) + ({}^{nv}\lambda)({}^{nn}\lambda) = 0. \tag{40}$$

With a given rotation matrix $\boldsymbol{U}$, let $\mathcal{L}(\boldsymbol{U})$ denote the set of $\boldsymbol{K}$s which satisfy (39), and $\mathcal{M}(\boldsymbol{U})$ denote the set of $\boldsymbol{K}$s which satisfy (39) and (40). Moreover, let $\mathcal{F}$ be the union of all $\mathcal{L}(\boldsymbol{U})$s, and $\mathcal{G}$ be the union of all $\mathcal{M}(\boldsymbol{U})$s. These relations are illustrated in Figure 5.

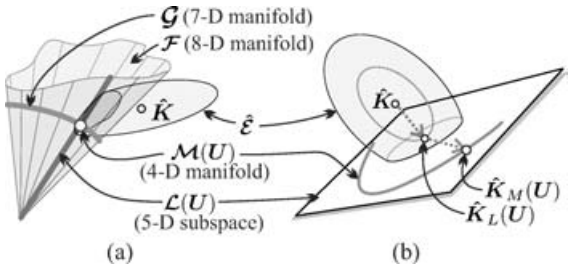


Fig. 5. Inclusive relationship among subsets of $\{\boldsymbol{K} \in \mathcal{R}^{3\times3}\}$.

https://doi.org/10.1017/S0263574704000918 Published online by Cambridge University Press

4.2. New estimate $\hat{\mathcal{E}}_M(\boldsymbol{U})$ with respect to a given $\boldsymbol{U}$

Since $\hat{\boldsymbol{K}}$ is generally not included in $\mathcal{G}$, we have to obtain an element of $\mathcal{G}$ which is close to $\hat{\boldsymbol{K}}$. For this purpose, this subsection provides a method to obtain an element of $\mathcal{M}(\boldsymbol{U})$ which is close to $\hat{\boldsymbol{K}}$. Hereafter, $(\boldsymbol{U})$ is omitted unless required for clarity.

We derive the element of $\mathcal{L}$ that minimizes $D(\boldsymbol{K})$, hereafter $\hat{\boldsymbol{K}}_L$. Let $\boldsymbol{L} \triangleq [\,\boldsymbol{n} \otimes \boldsymbol{U} \,|\, \boldsymbol{v} \otimes [\boldsymbol{n}, \boldsymbol{v}]\,]$ $(\in \mathcal{R}^{9\times 5})$ and $\boldsymbol{\lambda} \triangleq [{}^{nn}\lambda, {}^{tn}\lambda, {}^{vn}\lambda, {}^{nv}\lambda, {}^{vv}\lambda]^T$ $(\in \mathcal{R}^5)$. Then, when $\boldsymbol{K}$ is included in $\mathcal{L}$, it is correspondent to $\boldsymbol{\lambda}$ in the sense that $\mathrm{vec}[\boldsymbol{K}] = \boldsymbol{L}\boldsymbol{\lambda}$. By using $\boldsymbol{\lambda}$, $D(\boldsymbol{K})$ can be written as

$$D(\boldsymbol{K}) = (\boldsymbol{\lambda} - \hat{\boldsymbol{\lambda}}_L)^T {\boldsymbol{V}_L}^{-1}(\boldsymbol{\lambda} - \hat{\boldsymbol{\lambda}}_L) + \hat{D}_L \tag{41}$$

$$\hat{\boldsymbol{\lambda}}_L \triangleq \boldsymbol{V}_L \boldsymbol{L}^T \boldsymbol{\Pi}^{-1} \mathrm{vec}[\hat{\boldsymbol{K}}] \tag{42}$$

$$\hat{D}_L \triangleq \mathrm{vec}[\hat{\boldsymbol{K}}]^T \boldsymbol{\Pi}^{-1} \mathrm{vec}[\hat{\boldsymbol{K}}] - {\hat{\boldsymbol{\lambda}}_L}^T \boldsymbol{L}^T \boldsymbol{\Pi}^{-1} \mathrm{vec}[\hat{\boldsymbol{K}}], \tag{43}$$

where $\boldsymbol{V}_L \triangleq (\boldsymbol{L}^T \boldsymbol{\Pi}^{-1} \boldsymbol{L})^{-1}$. $\hat{\boldsymbol{\lambda}}_L$ corresponds to $\hat{\boldsymbol{K}}_L$ in the sense that $\mathrm{vec}[\hat{\boldsymbol{K}}_L] = \boldsymbol{L}\hat{\boldsymbol{\lambda}}_L$, and $\hat{D}_L$ is the generalized distance between $\hat{\boldsymbol{K}}_L$ and $\hat{\boldsymbol{K}}$. The generalized distance from $\hat{\boldsymbol{\lambda}}_L$ to $\boldsymbol{\lambda}$ is defined by $D_L(\boldsymbol{\lambda}) \triangleq (\boldsymbol{\lambda} - \hat{\boldsymbol{\lambda}}_L)^T {\boldsymbol{V}_L}^{-1}(\boldsymbol{\lambda} - \hat{\boldsymbol{\lambda}}_L)$, based on the crosssection ellipsoid of $\hat{\boldsymbol{\mathcal{E}}}$ with $\mathcal{L}$. Note that $\hat{D}_L$, $\boldsymbol{V}_L$, and $\hat{\boldsymbol{\lambda}}_L$ are functions of $\boldsymbol{U}$.

Next, we derive an element of $\mathcal{M}$ which is close to $\hat{\boldsymbol{K}}_L$ (i.e., at which $D_L(\boldsymbol{\lambda})$ takes a small value), hereafter $\hat{\boldsymbol{K}}_M$. Let the left-hand side of 40 be denoted by $a(\boldsymbol{\lambda})$, i.e., $a(\boldsymbol{\lambda}) \triangleq ({}^{vn}\lambda)({}^{vv}\lambda) + ({}^{nv}\lambda)({}^{nn}\lambda)$. Then, $a(\boldsymbol{\lambda})$ can be written in the form of $a(\boldsymbol{\lambda}) = \boldsymbol{\lambda}^T \boldsymbol{A} \boldsymbol{\lambda}$, where $\boldsymbol{A}$ is a symmetric 5×5 matrix. In the neighborhood of $\hat{\boldsymbol{\lambda}}_L$, $a(\boldsymbol{\lambda})$ can be approximated by

$$a(\boldsymbol{\lambda}) \approx \tilde{a}(\boldsymbol{\lambda}) \triangleq (2\boldsymbol{A}\hat{\boldsymbol{\lambda}}_L)^T (\boldsymbol{\lambda} - \hat{\boldsymbol{\lambda}}_L) + {\hat{\boldsymbol{\lambda}}_L}^T \boldsymbol{A} \hat{\boldsymbol{\lambda}}_L. \tag{44}$$

One can find that under the condition $\tilde{a}(\boldsymbol{\lambda}) = 0$, $\boldsymbol{\lambda}$ which minimizes $D_L(\boldsymbol{\lambda})$ can be expressed by $\boldsymbol{\lambda} = \hat{\boldsymbol{\lambda}}_L + x\boldsymbol{V}_L \boldsymbol{A} \hat{\boldsymbol{\lambda}}_L$ where x is a certain real number. Hence, $\hat{\boldsymbol{\lambda}}_M$ is defined as a $\boldsymbol{\lambda}$ which can be expressed in this form and that satisfies $a(\boldsymbol{\lambda}) = 0$. This is found by solving the second order equation $a(\hat{\boldsymbol{\lambda}}_L + x\boldsymbol{V}_L \boldsymbol{A} \hat{\boldsymbol{\lambda}}_L) = 0$ with respect to x. By this means, we can obtain $\hat{\boldsymbol{\lambda}}_M$ and $\hat{\boldsymbol{K}}_M$ (given by $\mathrm{vec}[\hat{\boldsymbol{K}}_M] = \boldsymbol{L}\hat{\boldsymbol{\lambda}}_M$).

The generalized distance between $\hat{\boldsymbol{K}}$ and $\hat{\boldsymbol{K}}_M$ is $\hat{D}_M \triangleq D(\hat{\boldsymbol{K}}_M) = \hat{D}_L + D_L(\hat{\boldsymbol{\lambda}}_M)$. The uncertainty ellipsoid accompanied by $\hat{\boldsymbol{K}}_M$, denoted by $\hat{\boldsymbol{\mathcal{E}}}_M$, can be given by moving $\hat{\boldsymbol{\mathcal{E}}}$ from $\hat{\boldsymbol{K}}$ to $\hat{\boldsymbol{K}}_M$, and magnifying it by $(1 + \hat{D}_M)$ times, in the same way as the determination of $\hat{\boldsymbol{\mathcal{E}}}_N(\boldsymbol{U})$ described in subsection 3.2. The elements of $\hat{\boldsymbol{\lambda}}_M$ and $\boldsymbol{V}_L$ are denoted by, for example, ${}^{nn}\hat{\lambda}_M$ and ${}^{nn,nn}V_L$.

4.3. Consistency evaluation of $\hat{\mathcal{E}}_M(\boldsymbol{U})$

When a given $\boldsymbol{U}$ is close to the true value, the ellipsoid $\hat{\boldsymbol{\mathcal{E}}}_M(\boldsymbol{U})$ is supposed to be consistent with the kinetic friction state on a cylindrical surface whose primary directions are $\boldsymbol{t}$ and $\boldsymbol{v}$. Equations (39) and (40) are conditions for the consistency of $\hat{\boldsymbol{\mathcal{E}}}_M(\boldsymbol{U})$, but more conditions are required. For example, (38) implies that ${}^{nn}\hat{\lambda}_M(\boldsymbol{U})$ and ${}^{vv}\hat{\lambda}_M(\boldsymbol{U})$ should be positive and negative, respectively. As well, we have to note that the IPA usually provides estimates with small uncertainties in directions in which the variance of position is large. This direction is usually close to the direction of motion, and must be consistent with the value of α. Moreover, we have to note that the estimates are consistent with the analytically derived (38) only under limited conditions. This is because (38) is based on the derivatives of the non-linear force-position relations, (35), (36), and (37), despite that the estimation is performed based on sensor observations distributed in a finite volume of space.

Based on the above consideration, we define a scholar function $\Phi(\boldsymbol{U})$ as follows:

$$\begin{aligned}
\Phi(\boldsymbol{U}) &= \beta^2 \Phi_{t1} \Phi_{t2} \Phi_{t3} + \Phi_{v1} \Phi_{v2} \Phi_{v3} \\
\Phi_{t1}(\boldsymbol{U}) &\triangleq {}^{tn}\hat{\lambda}_M(\boldsymbol{U})^2 / ({}^{tn}\hat{\lambda}_M(\boldsymbol{U})^2 + {}^{vn}\hat{\lambda}_M(\boldsymbol{U})^2) \\
\Phi_{t2}(\boldsymbol{U}) &\triangleq \frac{\max(0, ({}^{nn}\hat{\lambda}_M(\boldsymbol{U})))^2}{(1 + \hat{D}_M(\boldsymbol{U}))({}^{nn,nn}V_L(\boldsymbol{U}))} \\
\Phi_{t3}(\boldsymbol{U}) &\triangleq ((\boldsymbol{t} \otimes \boldsymbol{t})^T \boldsymbol{\Pi}^{-1} (\boldsymbol{t} \otimes \boldsymbol{t}))/(1 + \hat{D}_M(\boldsymbol{U})) \\
\Phi_{v1}(\boldsymbol{U}) &\triangleq {}^{vn}\hat{\lambda}_M(\boldsymbol{U})^2 / ({}^{tn}\hat{\lambda}_M(\boldsymbol{U})^2 + {}^{vn}\hat{\lambda}_M(\boldsymbol{U})^2) \\
\Phi_{v2}(\boldsymbol{U}) &\triangleq \frac{\min(0, ({}^{vv}\hat{\lambda}_M(\boldsymbol{U})))^2}{(1 + \hat{D}_M(\boldsymbol{U}))({}^{vv,vv}V_L(\boldsymbol{U}))} \\
\Phi_{v3}(\boldsymbol{U}) &\triangleq ((\boldsymbol{v} \otimes \boldsymbol{t})^T \boldsymbol{\Pi}^{-1} (\boldsymbol{v} \otimes \boldsymbol{t}))/(1 + \hat{D}_M(\boldsymbol{U})).
\end{aligned} \tag{45}$$

The above criterions can be explained as follows:

- The ratio between Φ_{t1} and Φ_{v1} corresponds to the value of α, which represents the direction of motion. It is expected that $\Phi_{t1} \approx \cos^2 \alpha$ and $\Phi_{v1} \approx \sin^2 \alpha$. Φ_{t1} has a large value when the motion is along the true $\boldsymbol{t}$ direction. Contrary to this, Φ_{v1} has a large value when the motion is along the true $\boldsymbol{v}$ direction.
- Φ_{t2} is a reliability measure of the condition ${}^{nn}\hat{\lambda}_M > 0$. When the motion is along the true $\boldsymbol{t}$-direction, the absolute value of ${}^{v}p$ in (35) is small. In this case, (35) is almost linear with respect to ${}^{n}p$, and thus ${}^{nn}\hat{\lambda}_M$ becomes significantly positive. When the motion is along the true $\boldsymbol{v}$-direction, on the other hand, due to the non-linearity of (35), ${}^{nn}\hat{\lambda}_M(\boldsymbol{U}) \approx \kappa > 0$ may or may not hold. This is the reason why the criterion Φ_{t2} is weighted by Φ_{t1}.
- Φ_{v2} is a reliability measure of the condition ${}^{vv}\hat{\lambda}_M < 0$. When the motion is along the true $\boldsymbol{v}$-direction, ${}^{vv}\hat{\lambda}_M$ becomes reliably negative. On the other hand, when the motion is along the true $\boldsymbol{t}$-direction, ${}^{vv}\hat{\lambda}_M$ becomes uncertain and unstable due to the small position variance in the $\boldsymbol{v}$ direction. Especially, when the surface is soft, the end-effector may be constrained in the $\boldsymbol{v}$ direction by the hollowed surface, and thus it is even possible that ${}^{vv}\hat{\lambda}_M$ may have a large positive value. For this reason the criterion Φ_{v2} is weighted by Φ_{v1}.
- Φ_{t3} and Φ_{v3} are inverses of the uncertainties accompanied by ${}^{tt}\hat{\lambda}_M = (\boldsymbol{t} \otimes \boldsymbol{t})^T \mathrm{vec}\boldsymbol{K}$ and ${}^{tv}\hat{\lambda}_M = (\boldsymbol{v} \otimes \boldsymbol{t})^T \mathrm{vec}\boldsymbol{K}$, respectively. ${}^{tt}\hat{\lambda}_M$ and ${}^{tv}\hat{\lambda}_M$ are equal to zero by definition (see (38)), but their accompanying uncertainties are influenced by the direction of motion. When the motion is along the true $\boldsymbol{t}$ direction, ${}^{tt}\hat{\lambda}_M$ has a small uncertainty due to the large position variance in the $\boldsymbol{t}$ direction, and thus Φ_{t3} becomes large. On the other hand, when the motion

https://doi.org/10.1017/S0263574704000918 Published online by Cambridge University Press

is along the true $\boldsymbol{v}$ direction, ${}^{tv}\hat{\lambda}_M$ accompanies a small uncertainty, and as a result Φ_{v3} becomes large.

- β is a small positive number for maintaining balance between Φ_{t2} and Φ_{v2}. This is necessary because Φ_{t2}'s value during motion in the true $\boldsymbol{t}$ direction is much larger than Φ_{v2}'s value during motion in the true $\boldsymbol{v}$ direction. Since (38), the ratio between the analytical values of ${}^{vv}\lambda$ and ${}^{nn}\lambda$ is $({}^{n}\hat{p})/(R-{}^{n}\hat{p})$, and β should be set roughly correspondent with this. However, since the precise value of $({}^{n}\hat{p})/(R-{}^{n}\hat{p})$ is unknown in advance, the determination of β is a somewhat difficult problem. β should be small because usually the depth $({}^{n}\hat{p})$ is much smaller than the curvature radius R. A too large β causes insensitivity to the curvature in the direction of motion, and a too small β results in oversensitivity to small oscillations of the force derived from stick-slip or small irregularities of the surface. In the experiments described in section 6, we set $\beta = 0.1$ through trial and error.

When the motion is along the true $\boldsymbol{t}$ direction, the first term of (45) becomes dominant. When the motion is along the true $\boldsymbol{v}$ direction, on the other hand, the second term of (45) becomes dominant.

By finding $\boldsymbol{U}$ which maximizes $\Phi(\boldsymbol{U})$, we can obtain the estimate of $\boldsymbol{U}$, to be denoted by $\hat{\boldsymbol{U}}$. The steepest gradient method is employed to calculate $\hat{\boldsymbol{U}}$.

4.4. Estimating κ, μ, and R

The stiffness coefficient, the friction coefficient, and the curvature can be estimated by using $\hat{\boldsymbol{U}}$, $\boldsymbol{V}_F \triangleq \boldsymbol{V}_L(\hat{\boldsymbol{U}})$ and $\hat{\boldsymbol{K}}_G \triangleq \hat{\boldsymbol{K}}_M(\hat{\boldsymbol{U}})$.

The stiffness coefficient, κ, can be estimated as $\hat{\kappa} = {}^{nn}\hat{\lambda}_G$, since (38). This is valid only when the motion is almost along $\boldsymbol{v}$ direction, because otherwise (35) becomes highly non-linear with respect to ${}^{n}p$.

Next, (38) implies that the friction coefficient, μ, is estimated as

$$\hat{\mu} = \sqrt{({}^{nt}\hat{\lambda}_G)^2 + ({}^{nv}\hat{\lambda}_G)^2}/|{}^{nn}\hat{\lambda}_G|. \tag{46}$$

Its uncertainty bound of $\hat{\mu}$ is given by

$$(\mu - \hat{\mu})^2 \leq \left(\frac{\partial\hat{\mu}}{\partial\hat{\boldsymbol{\lambda}}_G{}^T}\right)^T \boldsymbol{V}_F \left(\frac{\partial\hat{\mu}}{\partial\hat{\boldsymbol{\lambda}}_G{}^T}\right). \tag{47}$$

Finally, by using (38) again, the curvature, $\rho \triangleq 1/R$, can be estimated as

$$\hat{\rho} = (({}^{n}\hat{p}) - \kappa({}^{n}\hat{p})/({}^{vv}\hat{\lambda}_G))^{-1}. \tag{48}$$

Here, ${}^{n}\hat{p}$ is unknown. However, by using the normal force applied to the environment, to be denoted by $\hat{N}$, and using ${}^{n}\hat{p} = \hat{N}/\kappa$, we can estimate $\hat{\rho}$ as $\hat{\rho} = (\hat{N}/\kappa - \hat{N}/({}^{vv}\hat{\lambda}_G))^{-1}$. Due to the non-linearity of (37), this is valid only when the variance of ${}^{v}p$ is small. Moreover, one must note that $\hat{N}$ is the normal force applied to the surface, and cannot be derived from the sensor observation at that instant. Therefore, in order to estimate the curvature, the stiffness of the surface must also be known. The uncertainty of $\hat{\rho}$ can be defined in the same way as (47).

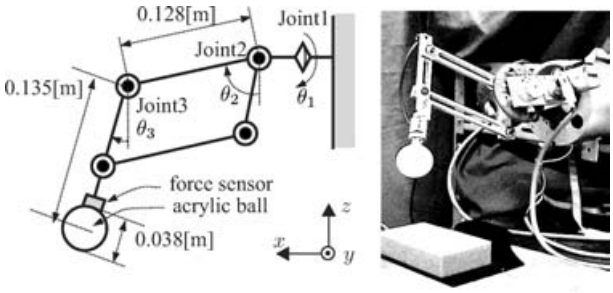


Fig. 6. Experiment I.

5. EXPERIMENT I (FLAT SURFACE)

5.1. Setup and method

This section describes preliminary experiments to test the method for recognizing flat surfaces, explained in section 3. The overview of the setup is shown in Figure 6. It consists of a three-joint robot arm, a 6-axis force-torque sensor, and an acrylic ball (diameter 38[mm], a table tennis ball), which is used as an end-effector. The position of the end-effector is measured by the optical encoders on the joints.

Three types of surfaces are used: a sponge (**S**), an acrylic board (**A**), and a metal file (**F**). The surfaces are located in two different postures: a 30-degree-inclined (posture-**i**) and a horizontal (posture-**h**). Thus, in total six cases exist: **iA**, **iF**, **iS**, **hA**, **hF**, and **hS**. As shown in Figure 7, the end-effector is moved along a semicircular target trajectory, using ordinary PD control in Cartesian space. When the target position is below the surface, the end-effector is slid on the surface and a compliant force is applied to the surface.

The sampling period of the IPA is 2[msec], and that of the surface property estimation is 10[msec]. The stiffness and viscosity of the VSF, K_{v} and B_{v}, are set to be 700[N/m] and 10[Ns/m], respectively. The weightings of the measurements ($w_{k,i}$ in (6)) are reduced to half after the 1.0×10^{-3}[m] of distance or 0.1[sec] of time is moved or elapsed. These parameters are designed by trial and error.

The friction coefficients of the surfaces **A**, **F**, and **S** are approximately 0.15, 0.45, and 0.41, respectively. The surfaces **A** and **F** are almost rigid, thus the apparent stiffness estimated through the VSF is expected to be equal to $K_{\mathrm{v}} = 700$[N/m]. The stiffness coefficient of the surface **S** is approximately 260[N/m], thus its apparent stiffness is expected to be $260K_{\mathrm{v}}/(260 + K_{\mathrm{v}}) \approx 189$[N/m].

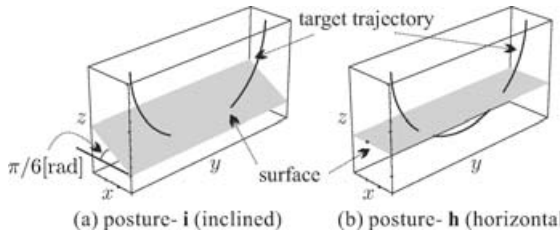


Fig. 7. Surface postures and target trajectories (Experiment I).

https://doi.org/10.1017/S0263574704000918 Published online by Cambridge University Press

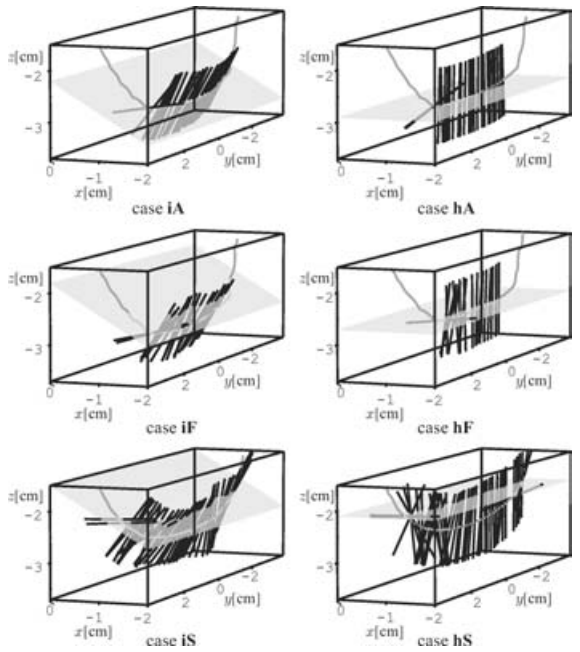


Fig. 8. Estimated normal direction $\hat{\boldsymbol{n}}$ (Experiment I).

5.2. Results

Figure 8 shows the estimated normal direction, $\hat{\boldsymbol{n}}$, and the trajectory of the end-effector, $\boldsymbol{p}_{\mathrm{r}}(t)$. The transparent planes represent the position of the object surfaces by actual measurement. On the other hand, Figure 9 shows the estimated stiffness and friction coefficients, $\hat{\kappa}$ and $\hat{\mu}$. Estimated values are represented by black solid curves and the uncertainties of the estimates by gray bands. The time spans in which the end-effector is in touch with the surfaces are bounded by the vertical lines (representing the discontinuities detected by the IPA[12]). The proposed algorithm of the estimation of surface properties (described in section 3) is performed only when $\hat{\boldsymbol{\mathcal{E}}} \not\ni \boldsymbol{O}_{3\times 3}$, i.e., $\hat{\boldsymbol{k}}^T \boldsymbol{\Pi}^{-1} \hat{\boldsymbol{k}} > 1$. Thus, it is performed only when the end-effector is in touch with the surface. The position of the surface is adjusted so that the maximum force is around 1.8[N]. Thus, the lengths of the contact times vary by the surfaces.

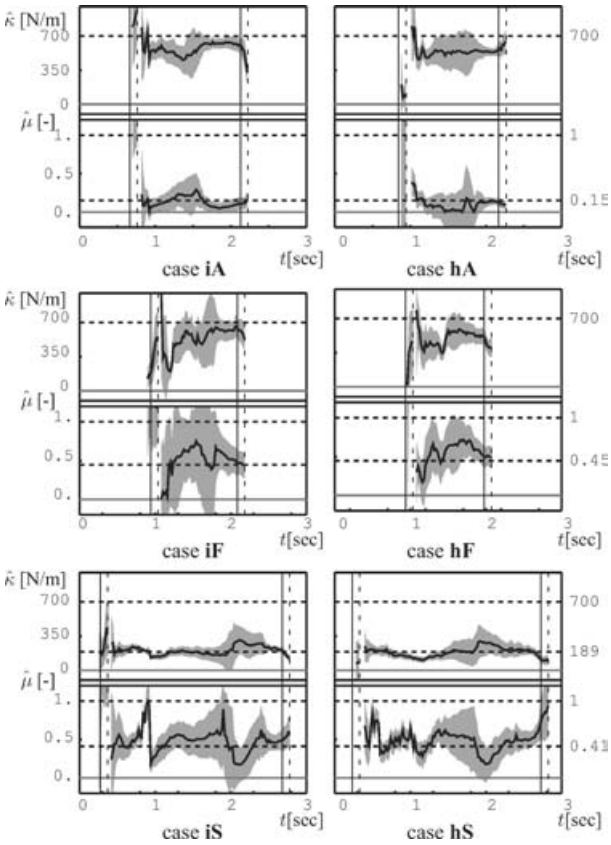


Fig. 9. Estimated stiffness and friction coefficients (Experiment I).

5.3. Discussion

Figure 8 shows that the normal directions are properly estimated, though the surface **S**, which is significantly deformed, slightly disturbs the estimations. Some misestimations follow the collisions, but these are limited to the short periods between when a discontinuity occurs and when that is detected.

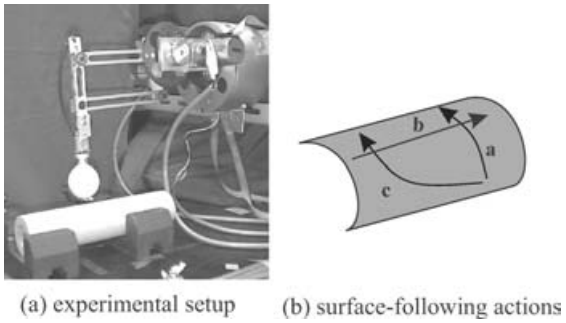
Figure 9 shows that, since the surfaces **A** and **F** are almost rigid, the stiffness coefficients, $\hat{\kappa}$, of **iA**, **hA**, **iF**, and **hF** are estimated to be large, around the VSF's limit $K_{\mathrm{v}} = 700$[N/m]. On the other hand, since the surface **S** is soft, $\hat{\kappa}$ in **iS** and **hS** have small values and they are close to 189[N/m] as expected. The friction coefficient, $\hat{\mu}$, of each surface is properly estimated. Those of surfaces **A** and **F** are distinctly different from each other. Same surfaces having different postures result in almost the same values of $\hat{\kappa}$ and $\hat{\mu}$. This indicates the validity of the proposed method.

6. EXPERIMENT II (CYLINDRICAL SURFACE)

6.1. Setup and method

This section describes preliminary experiments to test the method for recognizing cylindrical surfaces, which was explained in section 4. The experimental setup is the same as that is used in the previous section, but the robot is moved by the experimenter's hand without using the joint actuators.

We used two objects: **H** and **S**. Object **H** is a wooden cylinder (diameter 42[mm]), while object **S** is a soft cylindrical object (diameter 43[mm]) which consists of a wooden cylinder (diameter 24[mm]) covered with a soft sponge sheet (thickness 9[mm]). On each object, three surface-following actions, **a**, **b**, and **c**, were performed (see Figure 10b). Thus, in total six cases exist: **Ha**, **Hb**, **Hc**, **Sa**, **Sb**, and **Sc**.



(a) experimental setup (b) surface-following actions

Fig. 10. Experiment II.

https://doi.org/10.1017/S0263574704000918 Published online by Cambridge University Press

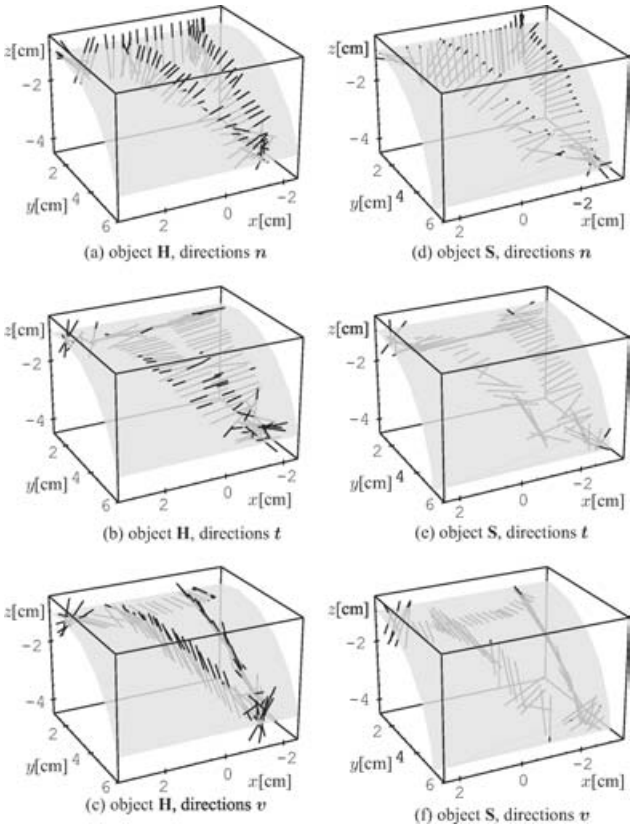


Fig. 11. Estimated directions $\hat{\boldsymbol{n}}$, $\hat{\boldsymbol{t}}$, and $\hat{\boldsymbol{v}}$ (Experiment II).

The sampling period of the IPA is 1.5[msec], and that of the surface property estimation is 15[msec]. The parameters of the VSF and the weighting rule of the measurements ($w_{k,i}$ in (6)) are set to be the same as those in Experiment I.

The friction coefficients of **H** and **S** are approximately 0.27 and 0.85, respectively, and the stiffness coefficient of **S** is approximately 320[N/m]. Object **H** can be regarded as rigid. The apparent stiffness coefficients of **H** and **S** estimated through the VSF are expected to be approximately $K_{\mathrm{v}} = 700$[N/m] and $320K_{\mathrm{v}}/(K_{\mathrm{v}} + 320) \approx 220$[N/m], respectively. Considering the radius of the end-effector, the estimates of the curvatures are expected to be $2/(42 + 38[\mathrm{mm}]) \approx 25[\mathrm{m}^{-1}]$ and $2/(43 + 38[\mathrm{mm}]) \approx 25[\mathrm{m}^{-1}]$, respectively.

6.2. Results

Figure 11 shows the estimated $\hat{\boldsymbol{n}}$, $\hat{\boldsymbol{t}}$, and $\hat{\boldsymbol{v}}$ and the actual positions of the objects (represented by the transparent surfaces). Figure 12 shows the estimated stiffness coefficient, ${}^{nn}\hat{\lambda}_G$, friction coefficient, $\hat{\boldsymbol{\mu}}$, and curvature, $\hat{\boldsymbol{\rho}}$. In Figure 12, the estimated values are represented by black solid curves and the uncertainties of the estimated values are represented by gray bands. The time spans in which the end-effector is in touch with the surfaces are bounded by vertical lines (representing the discontinuities detected by the IPA[12]. The estimation is performed only when the observed force is larger than a threshold. When the recursive computation is not completed within the sampling period (15[msec]), estimates are not obtained and blanks appear in the graphs.

6.3. Discussion

Figure 11 shows that $\boldsymbol{n}$, $\boldsymbol{t}$, and $\boldsymbol{v}$ are properly estimated in most cases. The estimates are stable and correct, especially, those regarding the non-deformable object **H**. Some misestimations follow the collisions, but most of them are limited to the short periods between the occurrence and the detection of the discontinuities. However, on the deformable object **S**, $\boldsymbol{t}$ and $\boldsymbol{v}$ are confused when the motion is not along primary directions, i.e., in action **c**. This indicates that the criterion $\Phi(\boldsymbol{U})$ may need reconsideration.

${}^{nn}\lambda$, correspondent to κ, is estimated to be close to the correct value under action **b**, along the primary direction $\boldsymbol{t}$. The cause of the incorrect estimations in actions **a** and **c** is as explained in 4.4. Nonetheless, the incorrect estimate with small uncertainty is an inappropriate output. This is an important problem to be solved.

The friction coefficient, μ, is correctly estimated especially under action **b**. It is appropriate that incorrect estimates accompany large uncertainties, but sometimes large uncertainties are obtained even when the estimate is near the true value. The definition of the uncertainty may have to be improved.

The estimation of ρ is performed only when ${}^{vv}\hat{\lambda}_G < 0$. As shown in (48), the stiffness κ and the normal force $\hat{N}$ are required to estimate ρ. $\kappa = 700$[N/m] is used for object **H**, and $\kappa = 220$[N/m] for object **S**. Due to the negligible weight of the end-effector, the observed force is directly used as $\hat{N}$. Figure 12 indicates that ρ is properly estimated in actions **a** and **c**, but the estimate is indeterminate in action **b**.

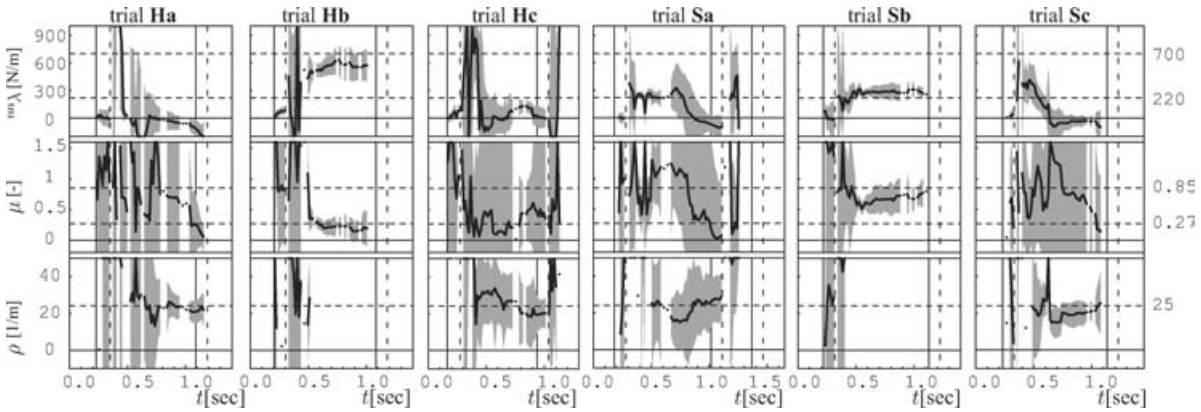


Fig. 12. Estimated stiffness coefficient ${}^{nn}\hat{\lambda}_G$, curvature $\hat{\rho}$, and friction coefficient $\hat{\mu}$ (Experiment II).

https://doi.org/10.1017/S0263574704000918 Published online by Cambridge University Press

On the whole, although the proposed method still has some aspects that need to be improved, it has been shown to have the potential for providing information regarding various surface properties.

7. CONCLUSION

This paper proposed methods for recognizing certain properties of flat and convex cylindrical surfaces, based on the stiffness matrix provided by the impedance perception algorithm (IPA)[12]. The methods were tested experimentally. The method intended for flat surfaces gave fair results, while the results for the method intended for cylindrical surfaces indicated that this method needed improvement. On the whole, the stiffness matrix obtained by the IPA was shown to be a potential source of information regarding various surface properties. Further enhancement will be required for general, both convex and concave, surfaces, and, moreover, for two or more constraint hypersurfaces.

In this paper we focused on information extraction from very short time period. As a future direction of research, data aggregation in time and space dimensions should be considered. Temporal aggregation will improve the estimation's reliability by trading off responsiveness. Spatial aggregation of the data will be necessary to construct a global model of the environment.

Though the main purpose of this method is to obtain qualitative information including uncertainty, the precision and accuracy of the estimation must be evaluated quantitatively. The influences of the design parameters on the estimation accuracy must be clarified, especially for an optimal design of the forgetting factors and the VSF. This will also be a future topic of study.

References

1. T. Yoshikawa, Y. Yu and M. Koike, "Estimation of Contact Position between Object and Environment Based on Probing of Robot Manipulator," *Proceedings of the 1996 IEEE/RSJ International Conference on Intelligent Robots and Systems* **2**, (1996) **Vol. 2**, pp. 769–776.
2. T. Mouri, T. Yamada, N. Mimura and Y. Funahashi, "Identification of Contact Conditions from Contaminated Data of Contact Moment," *Proceedings of the 1999 IEEE International Conference on Robotics and Automation* (1999) pp. 585–591.
3. A. M. Okamura and M. R. Cutkosky, "Feature-Guided Exploration with a Robotic Finger," *Proceedings of the 2001 IEEE International Conference on Robotics and Automation* (2001) pp. 589–596.
4. B. Eberman and J. K. Salisbury, "Application of Change Detection to Dynamic Contact Sensing," *Int. J. Robotics Research* **13**(5), 369–394 (1994).
5. M. Skubic and R. A. Volz, "Identifying Single-Ended Contact Formations from Force Sensor Patterns," *IEEE Transactions on Robotics and Automation* **16**(5), 597–602 (2000).
6. B. J. McCarragher and H. H. Asada, "Qualitative Template Matching Using Dynamic Process Models for State Transition Recognition of Robotic Assembly," *Journal of Dynamic Systems, Measurement, and Control* **115**, 261–269 (1993).
7. G. E. Hovland and B. J. McCarragher, "Hidden Markov Models as a Process Monitor in Robotic Assembly," *Int. J. Robotics Research* **17**(2), 153–168 (1998).
8. G. E. Hovland, P. Sikka and B. J. McCarragher, "Skill Acquisition from Human Demonstration Using a Hidden Markov Model," *Proceedings of the 1996 IEEE International Conference on Robotics and Automation* (1996), pp. 2706–2711.
9. B. J. McCarragher, "Force Sensing from Human Demonstration Using a Hybrid Dynamical Model and Qualitative Reasoning," *Proceedings of the 1994 IEEE International Conference on Robotics and Automation* (1994), pp. 557–563.
10. M. Skubic and R. A. Volz, "Acquiring Robust, Force-Based Assembly Skills from Human Demonstration," *IEEE Transactions on Robotics and Automation* **16**(6), 772–781 (2000).
11. P. Dupont, T. M. Schuteis, P. A. Millman and R. D. Howe, "Automatic Identification of Environment Haptic Properties," *Presence* **8**(4), 394–411 (1999).
12. R. Kikuuwe and T. Yoshikawa, "Robot Perception of Environment Impedance," *Proceedings of the 2002 IEEE International Conference on Robotics and Automation* (2002), pp. 1661–1666.
13. M. Charlebois, K. Gupta and S. Payandeh, "Shape Description of Curved Surfaces Using Tactile Sensing and Surface Normal Information," *Proceedings of the 1997 IEEE International Conference on Robotics and Automation* (1997), pp. 2819–2824.
14. M. Moll and M. A. Erdmann, "Dynamic Shape Reconstruction Using Tactile Sensors," *Proceedings of the 2002 IEEE International Conference on Robotics and Automation* (2002), pp. 1636–1642.
15. Z. A. Parszewski, J. M. Krodkiewski and J. Rucinski, "Parametric Instabilities of Rotor-Support Systems with Asymmetric Stiffness and Damping Matrices," *Journal of Sound and Vibration* **109**, 111–125 (1986).
16. C. M. Jung and B. F. Feeny, "On the Discretization of an Elastic Rod with Distributed Sliding Friction," *Journal of Sound and Vibration* **252**, 409–428 (2002).

https://doi.org/10.1017/S0263574704000918 Published online by Cambridge University Press